Analysis of individual (macro)molecules and proteins using near-field optics

Niek F. van Hulst,[a] Joost-Anne Veerman, María F. García-Parajó, and L. (Kobus) Kuipers
Applied Optics Group, Faculty of Applied Physics & MESA+ Research Institute, University of Twente, P.O. Box 217, 7500 AE Enschede, The Netherlands

(Received 2 December 1999; accepted 1 February 2000)

Recent achievements in single molecule detection using near-field optical excitation are presented. By proper control of technology, distinct advantages of near-field optics are exploited: (i) the nanometric excitation/emission volume (10^4–10^5 nm^3), which provides high spatial resolution, localization of a single molecule within a few nm, and reduced background; (ii) the sensitivity for single molecule orientation in all three dimensions; (iii) the high local brightness, allowing real-time single molecule detection down to μs resolution; (iv) the simultaneous colocalization with nanometric surface topography. Real-time quantum jumps between singlet and triplet state of an individual molecule are observed. Distributions for triplet state lifetime and crossing yield are determined. Both triplet state lifetime and crossing yield of a single molecule appear to vary in time, due to the local heterogeneity. Individual dendritic molecules containing a single fluorescent core are investigated. The dendritic assemblies are discriminated from free fluorescent cores on the basis of accurate simultaneous localization of both the fluorescent core and the topography of the surrounding dendritic shell. Intramolecular rotational motion of the fluorescent core is observed. Individual green fluorescent proteins are visualized, both in fluorescence and topography. Photoinduced conformational changes to a nonemissive form of the protein are observed, leading to long dark intervals of several seconds. © *2000 American Institute of Physics.*
[S0021-9606(00)70216-9]

INTRODUCTION

In 1993 Betzig and Chichester[1] entered into the world of ''single molecule detection'' by the first observation of individual molecules at room temperature using near-field fluorescence microscopy. Until then, pioneering single molecule studies had been restricted to cryogenic temperatures.[2,3] Their achievement was soon followed by room-temperature experiments to reveal strongly dynamic processes.[4–6] Today single molecule fluorescence detection has evolved to a new frontier in science[7–13] with high impact and potential for a wide range of disciplines, such as material research, analytical chemistry, and the biological sciences.

Monitoring the fluorescent behavior of an individual molecule in time has essential advantages over ensemble-averaged experiments. Single molecule time trajectories exhibit stochastic fluctuations that directly contain detailed statistical and dynamical information of systems under equilibrium conditions. Time-dependent processes and reaction pathways in nonequilibrated systems can be followed and studied without the need for synchronizing a population of molecules. Single molecule detection reveals the full distribution of a given molecular property, instead of a statistical average. Thus, static and dynamic heterogeneity in a population of molecules in a complex condensed system can be identified and related to the molecular environment. As such, a single molecule can be viewed as a local reporter of its nanoenvironment. Finally, single molecule detection allows observation in real time of transient intermediates that are otherwise difficult to capture in ensemble experiments because of their low steady-state concentrations.

The mentioned advantages are illustrated by numerous remarkable single molecule observations over recent years. Single molecule (center-of-mass) translational motions have been studied on fluid lipid membranes[14] in polymer matrices,[15–17] along actin filaments,[18,19] and DNA.[20] Similarly orientational mobility[17,21–23] has been observed on a typical timescale of milliseconds to tens of seconds. Such experiments are useful to probe polymer mobility, membrane transport mechanisms, and dynamic interactions of macromolecules like proteins and DNA. Spectral diffusion at room temperature has been shown for the first time on single molecules.[24–26] The process is both photoinduced and thermally driven and provides a direct view on the potential energy landscape of the molecules. Correspondingly significant differences in fluorescence lifetimes have been found among seemingly identical molecules,[25,27,28] giving a detailed insight in the competition between radiative and nonradiative (quenching) rates[29,30] on the nanometer scale. For example, fluorescence lifetime has proven to be very sensitive to the proximity of an adjacent guanosine base in DNA-dye studies.[31–33] Currently the nanometric distance sensitivity of single pair fluorescence resonance energy transfer (FRET) is increasingly exploited to monitor conformational motions of individual, especially biological,

[a]Author to whom correspondence should be addressed. Electronic mail: n.f.vanhulst@tn.utwente.nl

macromolecules.[34,35] Multichromophoric systems, such as aggregates and multimeric complexes receive attention because of the potential excitonic (de)localization, which makes these systems behave as a single quantum system displaying discrete on/off switching.[36–39] Finally, single molecule studies are particularly useful to understand multiexponential chemical kinetics, e.g., due to variation in activation energy[40] or existence of an intermediate state.[41]

Among the various techniques that are used for single molecule fluorescence detection are near-field microscopy and far-field methods, such as confocal, wide-field, and total-internal-reflection (dark-field) microscopy. Lately, single molecule two-photon excitation,[42,43] surface plasmon excitation,[44] and surface-enhanced Raman spectroscopy (SERS)[45,46] have been reported.

The far-field methods have proven to be highly versatile, operating from cryogenic to ambient conditions, from controlled atmosphere to biological flow cells. Moreover, applying total-internal reflection and wide-field approaches, a large area of the sample can be illuminated, which allows simultaneous detection of several individual molecules, using a CCD camera. However, all far-field methods are intrinsically diffraction limited to an excitation/detection volume of $>10^8$ nm^3, which implies that only samples with very low concentration of fluorophores can be studied, typically >10 molecules/μm^2 on a surface. Furthermore, the lateral optical response of typically 300 nm implies a localization accuracy of 30–40 nm for an efficient fluorophore.[14,47]

In contrast, near-field optical microscopy offers distinct advantages over the far-field methods when applied to single molecule studies. For the case of near-field optical microscopy based on aperture probes, several benefits are of importance. First, the excitation/detection volume is 10^4–10^5 nm^3, i.e., more than three orders-of-magnitude smaller excitation volume, which allows independent observation of more closely packed molecules, typically $\sim$100 molecules/μm^2 on a surface. In addition the small excitation volume reduces considerably the background emission from the sample. A superior lateral optical response of $\sim$70 nm on a single molecule can be obtained, which results in a localization accuracy down to only a few nm.[48] Second, near-field excitation provides an intrinsic high sensitivity for the 3D orientation of the molecular transition dipole moment. This follows from the particular near-field excitation patterns that arise due to the presence of both lateral and longitudinal polarized electric fields close to the aperture and allow the determination of both lateral and vertical components of the molecular dipole moment.[1,17,49] Likewise the aperture probe is a source of evanescent fields, which enables to launch ''forbidden'' waves, such as a surface plasmon.[50] Third, near-field microscopy is a true scanning probe method. Thus optical and topographic molecular information are obtained simultaneously, which enables direct correlation of fluorescent and structural properties.[23,51–54] Finally, the scanning near-field probe can be used to actively manipulate and control the sample by e.g., a local electric field[55] or energy transfer.[56]

The first near-field optical observation of single molecule fluorescence in 1993 by Betzig and Chichester[1] stimulated the field of single molecule detection but also set a standard in near-field optics, especially with their 3D-orientation determination of single molecules. Subsequent near-field experiments involved single molecule spectra[24] and fluorescence lifetimes,[27,28] lateral diffusion and rotation in a polymer host,[15,17] single-pair FRET,[57] single fluorophore labeled DNA strands,[23,58] and green fluorescent proteins.[59] Yet, despite the potential of near-field optics, today almost all single-molecule fluorescence experiments are performed using far-field microscopy because of the much less complexity. The most critical element is the near-field probe itself, which proves to be difficult to fabricate reliably in high quality. The poor quality of the aperture makes it generally hard to reproduce the standard set by Betzig and Chichester.[1] Similarly the limited brightness of conventional aperture probes restricts the achievable power density and detectable fluorescence signal in single molecule experiments. In subsequent experiments it was shown that the fluorescence lifetime of a molecule in the presence of a probe is altered by competition between radiative and nonradiative (quenching) mechanisms at small ($<$20 nm) probe–molecule distances,[27–30] which may complicate quantitative interpretation. Finally, the sample must be kept within the near-field of the probe, for which vibration isolation and a feedback system with subnanometer accuracy must be implemented. As a result, technological obstacles and the complicating presence of a probe in close proximity to the molecule have directed current single molecule research towards far-field methods.

In this article, we demonstrate that the intrinsic advantages of near-field optics, that motivated the early single molecule researchers, can definitely be exploited in a wide range of disciplines simply by proper control of the technology. After a short description of instrumentation and fabrication of well-defined high-brightness aperture probes, we show that single molecules are excellently suited to investigate the optical near-field distribution of the near-field probe. Conversely the near-field allows accurate determination of the molecular location and orientation. Next, the method is applied to the observation of real-time singlet–triplet quantum jumps. Ultimately, the unique combination of subwavelength resolution and simultaneous topographic detection is applied to individual guest–host systems, dendritic molecules, and green fluorescent proteins, to study colocalization, intramolecular rotation, and photoinduced switching.

INSTRUMENTATION

All experiments described in this article have been performed with an aperture-type near-field scanning optical microscope (NSOM)[60–62] using fluorescence detection.[17,54] A near-field aperture probe acts as a subwavelength light source, which is scanned in close proximity over the sample surface. Detection of fluorescence from the sample is accomplished in transmission in the far-field using an objective for large angle collection. Decisive for the NSOM performance is the quality of the aperture probe and the regulation system for probe–sample feedback.

Many different concepts for aperture probes were explored during the past 15 years, each of them with distinct advantages.[60–64] Commonly a fiber is pulled to an apex of nanometer dimensions and coated with aluminum. However,

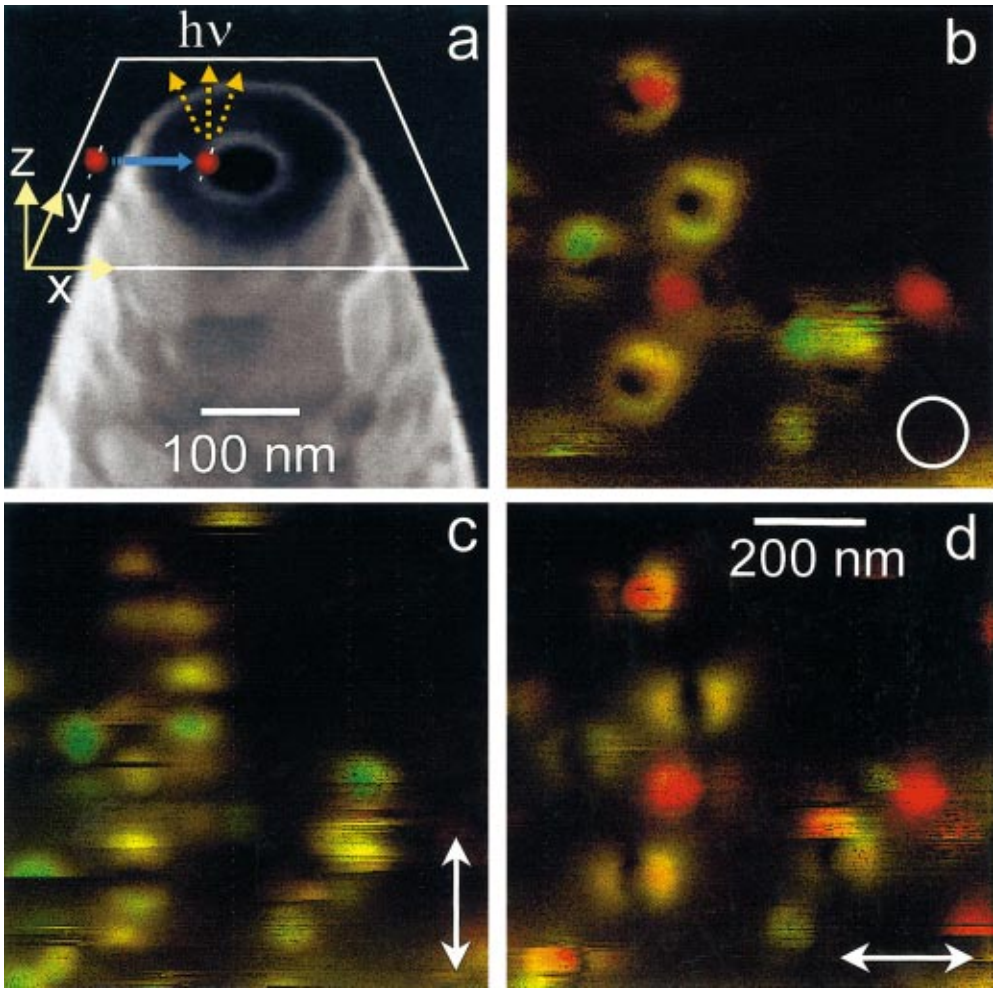

FIG. 1. (Color) (a) FIB image of a FIB-etched near-field aperture probe with aperture diameter 70(5) nm. The probe has a flat end-face and an aperture with well-defined edges and circular symmetry. The principle of near-field single molecule detection is sketched. A single molecule is scanned in the *x*-*y* plane parallel to the probe end-face and excited if the molecular absorption dipole moment matches the local field vector of the aperture field. Generated fluorescence is collected in the far-field. (b), (c), (d) Series of three NSOM fluorescence images of the same area of a sample of $DiIC_{18}$ molecules embedded in a 10 nm thin film of PMMA, as measured with the 70 nm aperture probe in (a). The fluorescence signal is color-coded red/green according to the detected *x*/*y* polarization. The excitation polarization was changed between circular (b), linear along the vertical *y*-direction (c), and linear along the horizontal *x*-direction (d). The 3D optical near-field distribution and the molecular dipole orientation determine the appearance of the molecules. Molecules oriented in *x*, *y*, and *z* direction are observed, where molecules oriented along *z* (out of plane) show up as circles and double lobes (Refs. 1 and 49).

probes that combine all necessary demands for NSOM have only scarcely been produced. Generally, the evaporated aluminum coating has a grainy structure, resulting in pinholes and an irregularly shaped aperture with asymmetric polarization behavior. Moreover, the grains increase the distance between aperture and sample, causing reduction of resolution and loss of local excitation intensity. Also the damage threshold of the coating generally limits the probe brightness to <10 nW in the far-field. In an refined approach, we have fabricated high definition aperture probes, combining superior polarization characteristics and high throughput, by making use of the focused ion beam (FIB) technique, which is capable of polishing on a nm scale.[48] In the FIB apparatus (FIB 200, FEI) a beam of Ga ions, collimated to 7 nm, is used to remove a very thin slice of material from the aluminum coated probe end. The resulting ''FIB probe'' has a flat-end face with a roughness below 7 nm and a well-defined circular aperture. Figure 1(a) shows a 70 nm aperture probe after FIB milling, as imaged in the FIB apparatus at low beam dose. We managed to fabricate apertures as small as 20 nm. The polarization extinction ratio exceeds 100:1 for all polarization directions. For single molecule studies we generally use 70 to 90 nm aperture probes with brightness up to 1 μW, corresponding to $\sim$20 kW/cm^2 at the molecule.

The distance between probe and sample is kept constant (nonzero) using a feedback on the force acting between probe and sample. Shear forces acting on the probe are picked up by a quartz tuning fork,[65] oscillating in resonance at 32 kHz, with $\sim$0.5 nm lateral amplitude at the probe end. Phase detection of the resonator response allows to establish a fast feedback loop,[66,67] with a set-point range for the distance between 2 and 25 nm. The force feedback generates a high-resolution topographical image with $\sim$0.2 nm residual vertical noise. Currently, the quality of topographic imaging in NSOM based on tuning forks approaches that of regular cantilever-based atomic force microscopy.[68]

The actual near-field optical microscope is integrated in a commercial inverted optical microscope (Zeiss Axiovert

135).[17,54] The commercial microscope sample stage is removed and replaced by a solid metal plate, supporting three tube piezoelectric elements (7 μm lateral scan range) arranged around the objective (Zeiss Neofluar 1.3 NA). The piezoelectric scanner is further linearized and stabilized (drift <1 nm/min) using a lateral position feedback system. The sample (generally a microscope cover glass) is kept by small magnets and supported by a stainless steel plate that fills most of the free volume between sample and objective, together with the immersion oil. Probe and tuning fork are mounted in a tripod system that allows fine approach and lateral manipulation for alignment with respect to the objective. Finally the whole microscope is suspended on springs to the ceiling to suppress residual vibrations below 0.1 nm amplitude (1 Hz–10 kHz).

A CW Ar^+/Kr^+ laser is used for availability of many wavelengths in the visible regime. A section of wave plates and prism polarizers allows control of the polarization that is coupled into the fiber. The fiber is kept short ($\approx$10 cm) in order to minimize background luminescence due to fiber dopants. Fluorescence is collected with the 1.3 NA objective, filtered from the excitation wavelength using long-pass filters, separated in two orthogonal polarization channels by a broadband polarizing beam-splitter and finally detected with two photon-counting avalanche photodiodes (APD, SPCM-100, EG&G Electro Optics). The collection efficiency was determined to be $\sim$10%, for an isotropic point source in the focus of the 1.3 NA objective. The main loss is at the limited angular collection efficiency (25%) of the objective and limited detection efficiency of the APD (55%). Of course, for single molecules with a nonisotropic radiation pattern, the collection efficiency is a function of the molecular orientation. Typically a fluorescence signal of 10^4-10^6 counts/s is detected from an individual molecule.

A personal computer controls the raster scanning of the sample using two D/A converters and collects the photocounts for each APD. Three images are collected simultaneously: a topographic image, and two optical fluorescence images. Moreover control signals for shear force and lateral position feedback are recorded. Alternatively the scanner is directed to a specific position (using the position feedback system) and fluorescence traces are recorded in time.

SINGLE MOLECULE ORIENTATION AND LOCALIZATION

The initial single molecule experiments by Betzig and Chichester[1] were performed on carbocyanine molecules immobilized on a polymer host. Carbocyanines are suitable ''test'' molecules due to their high fluorescence quantum yield and photostability (bleaching rate $10^{-6}-10^{-8}$). For first analysis of our probe performance we started with similar samples of carbocyanine ($DiIC_{18}$) molecules immobilized in a thin polymethyl–methacrylate (PMMA) layer.

$DiIC_{18}$ (Molecular Probes, D-282) was diluted in methanol (Merck, 99.8%) to a final concentration of 5×10^{-8} M. The dye solution was added to a 0.5% weight PMMA in toluene (Merck, 99.4%). A 10–20 μl drop was spin coated at 4000 rpm onto a 170 μm coverslip, resulting in a 5–10 nm layer with a surface coverage of typically $\sim$25 $DiIC_{18}$ molecules per square micrometer. The sample was excited at 514 nm wavelength and fluorescence $>$550 nm was detected.

Three sequential near-field fluorescence images are shown in Figs. 1(b)–1(d). The images were obtained with the 70 nm aperture probe of Fig. 1(a). The polarization of the excitation light was circular, linear along the *y*-direction and linear along the *x*-direction, respectively. Red/green indicates *x*/*y*-polarized fluorescence, respectively. Excitation by *y*-polarized light, in Fig. 1(c), gives mainly *y*-polarized fluorescence (green), because molecules with a large dipole component along the *y*-direction are selected. Similarly, in Fig. 1(d), *x*-polarized excitation yields mainly *x*-polarized fluorescence (red) by selecting *x*-oriented molecules. Clearly, a largely different set of molecules is selected by rotating the excitation polarization over 90°. It should be noted that the angle between absorption and emission transition moment is 28° for DiI,[69] therefore absorption and emission polarization characteristics should be taken into account separately. In Fig. 1(b), with circular excitation polarization, all in-plane dipole moments are excited equally and emission in various polarization directions is observed (green, yellow, and red) depending on the direction of the molecular emission moment. Most remarkable in Fig. 1(b) are the ring-shaped emission patterns that turn into double-lobed patterns in Figs. 1(c) and 1(d), with the lobes in the direction of the excitation polarization. These characteristic rings and lobes were first observed by Betzig and Chichester.[1] They originate from the nonzero near-field components in the *z*-direction, which occur at the glass–metal interface.[70,71] The *z*-field mainly excites molecules with their absorption moment perpendicular to the sample surface. As a consequence the polarization of the emission is circularly symmetric in the *x*/*y* plane, making these molecules show up as yellow.

Figures 1(b)–1(d) show single molecule patterns with unprecedented detail for an optical image. In fact, considering the relative size of molecule and aperture, it would be more correct to state that the images display the optical near-field distribution of an aperture probe with a single molecule as local detector [sketched in Fig. 1(a)]. The resolution is determined by the molecular absorption cross-section, while the dimensions of the field patterns are characteristic for the aperture probe. For the in-plane molecules the full width at half maximum (FWHM) of the patterns is 85(5) nm, in agreement with a 70 nm aperture and 15 nm distance between aperture and molecule, as estimated from the shear force feedback set-point. The width of the rings and lobes is 45(5) nm (FWHM), considerably smaller than the aperture size. This width is determined by the lateral extent of the *z*-fields at the aperture edge. A lower limit is the optical skin depth of aluminum (6.5 nm for green light). At 15 nm distance from the aperture edge a broadening to $\sim$30 nm is expected,[70] slightly below the observed width.

Detailed analysis of the molecular excitation/emission polarization patterns allows quantitative 3D determination of the molecular absorption and emission dipole orientation. Hereto the 3D optical near-field distribution, the molecular emission pattern, and the finite NA of the objective should be taken into account.[72]

Close inspection of Fig. 1 reveals molecular dynamic

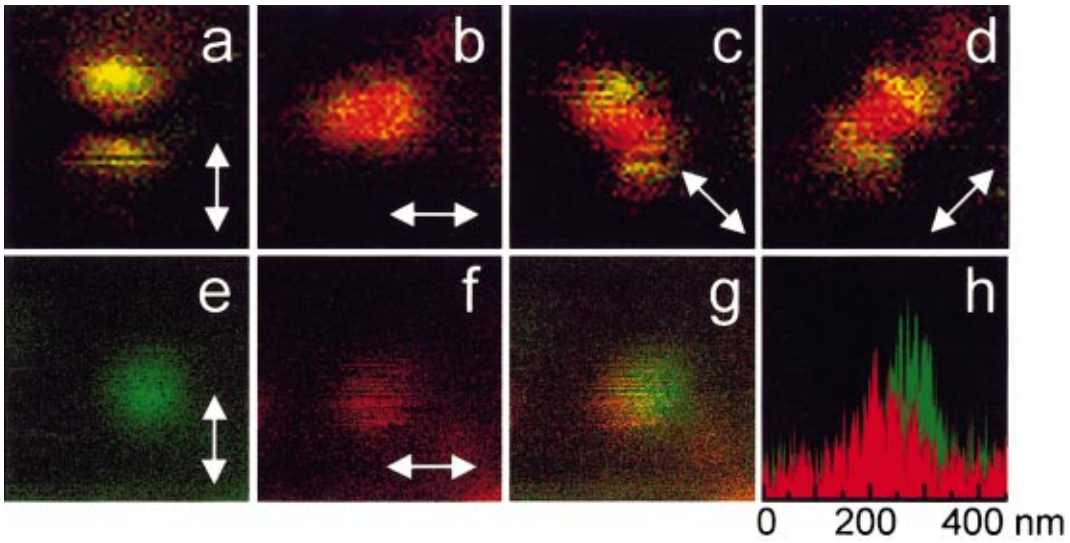

FIG. 2. (Color) Examples of near-field optical single molecule localization. (a)–(d) Series of four successive measurements of the same 440×440 nm sample area obtained with a 70 nm aperture probe. The fluorescence signal is color-coded red/green according to the detected x/y polarization. The linear excitation polarization direction was varied between (a) 90° y-direction, (b) 0° x-direction, (c) −45°, and (d) 45°. Two molecules are visible located within 10 nm from each other: one molecule in the sample plane along the x-direction [red in (b)], the other mainly perpendicular to the sample plane [yellow in (a)]. (e)–(f) Series of images for two other molecules. The linear excitation polarization direction was varied between (e) 90° y-direction and (f) 0° x-direction. Combination of images (e) and (f) in (g) shows discrimination of the two molecules, one along the x-direction (red), the other along the y-direction (green). In graph (h) line traces of the molecular fluorescence signal in both polarization channels are plotted, showing the two molecules separated by 45(10) nm.

effects, such as interrupted emission, discrete photodissociation, and occasional molecular rotation, which will be treated in more detail in the next section.

Clearly the near-field method allows to resolve closely packed individual molecules with ~70 nm resolution in a density up to 100 molecules/μm^2. What's more, the narrow near-field response function allows to locate single molecules with even higher accuracy, mainly limited by signal-to-noise. Figure 2 shows some specific examples of very closely spaced molecules that can still be discriminated. In Figs. 2(a)–2(d) a series of four measurements of a 440 ×440 nm^2 sample area is presented, obtained with a 70 nm aperture probe under various linear excitation polarization conditions (indicated by the arrows). Two molecules are visible: one molecule with a mainly in-plane orientation along the horizontal x-direction [red in Fig. 2(b)] and a second molecule oriented mainly perpendicular to the sample surface [yellow double-lobed near-field pattern in Fig. 2(a)]. The relative orientation of the double-lobed pattern follows the excitation polarization direction. The first molecule vanishes in Fig. 2(a) where the excitation polarization is perpendicular to its absorption dipole moment. Examination of the near-field distributions for both molecules reveals that their lateral position difference is smaller than 10 nm, corresponding to an optical localization accuracy $<\lambda/60$. Figures 2(e)–2(h) present a different case of two molecules, both oriented in plane: one molecule oriented along the vertical direction [green in Fig. 2(e)] the other along the horizontal direction [red in Fig. 2(f)]. The combined image is shown in Fig. 2(g), where the two molecules can be discriminated based on their different emission polarization. Obviously in this case the two-channel polarization detection prooves to be essential to distinguish the two molecules from a single emitter. A single molecule line profile is plotted in Fig. 2(h) for both polarization channels. A fit to the profiles yields a mutual distance of 45 nm within 10 nm accuracy.

The near-field single molecule localization accuracy should be directly confronted to the accuracy obtained for confocal single molecule detection. In confocal studies a lateral accuracy of 30 nm to 40 nm was reported,[14,17] corresponding to $\lambda/15$. The attainable accuracy for any optical detection method is basically determined by the signal-to-noise ratio, i.e., the number of collected photocounts, and the spatial response function of the microscopic method. For 10^4 collected counts an accuracy of 6 nm is achievable with a 70 nm probe, as compared to 30 nm for confocal detection with 1.3 NA. For 10^5 counts these values shift to 3 and 15 nm, for near-field and confocal detection, respectively. In the axial direction the near-field amplitude decreases dramatically with increasing distance from the aperture[71] yielding distance sensitivity within a few nanometers, as compared to ~100 nm accuracy[47] along the axis of a tight focus.

FLUCTUATIONS IN INTERSYSTEM CROSSING DYNAMICS

The FIB probes provide a power density of 20 kW/cm^2 on an area with ~70 nm in diameter. For efficient organic dye molecules this power density is close to the saturation of the obtainable absorption–emission photon cycle. For example, using FIB probe excitation, we managed to collect up to ~10^6 counts/s from an individual $DiIC_{18}$ molecule, corresponding to ~10^7 photons/s. We have exploited this high single molecular photon flux to observe time-resolved intersystem crossing dynamics for individual molecules at room temperature. Real-time fluorescence traces, covering many seconds at 30 μs integration time, were recorded for $DiIC_{18}$ molecules embedded in different types of polymer.[73]

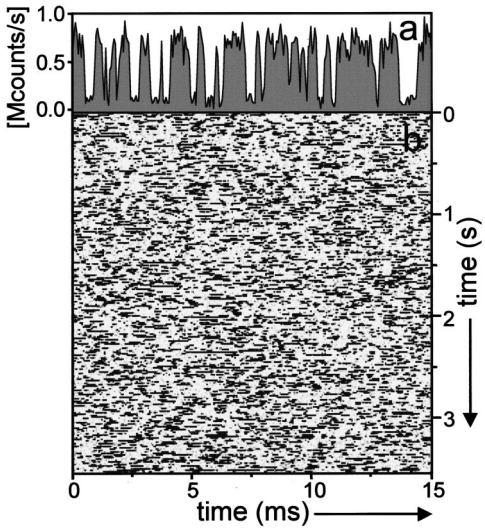

FIG. 3. (a) Single molecule fluorescence time trace with 57 μs integration time per point. The fluorescence drops repeatedly to a low level. This characteristic switching between ''on'' and ''off'' (blinking) corresponds to the molecule jumping between singlet and triplet state, respectively. (b) Real-time-image with 3.5 s of fluorescence blinking. Time runs continuously from line to line (left⇒right,top⇒bottom). The gray level represents the photon count rate during a 57 μs bin: bright streaks are due to the S_0-S_1 singlet excitation–emission cycle; dark streaks represent residence in the T_1 triplet state. Several thousands of triplet excursions occur during the 3.5 s observation time.

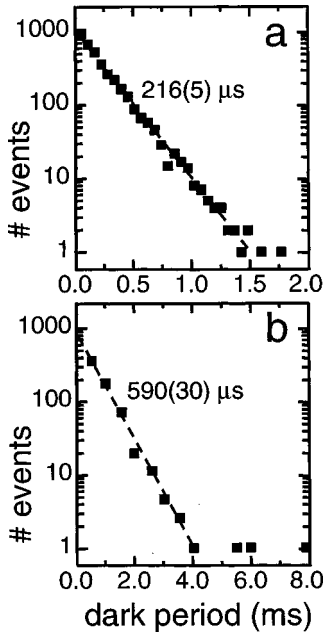

FIG. 4. (a) Histogram of the length of the ''dark'' periods for a single $DiIC_{18}$ molecule over an observation time of 2.8 s. The monoexponential decay corresponds to a mean T_1 lifetime of 216(5) μs. (b) Monoexponential decay of the dark period distribution for another molecule, with 590(30) μs T_1 lifetime. Moreover single dark events occur with intervals up to 8 ms, far beyond triplet statistics.

The experimental approach is similar to near-field optical microscopy. First, an image of the spatial distribution of a set of molecules is recorded. Next, the molecular positions are determined with nanometric accuracy. Finally, the near-field source is positioned directly above a selected molecule and the fluorescence is monitored continuously as a function of time, until irreversible photobleaching occurs.

Figure 3(a) shows a 15 ms trace of the real-time evolution of the fluorescence of a single $DiIC_{18}$ molecule embedded in PMMA. Clearly the emission shows a discrete high (''on'') and low (''off'') intensity level. The abrupt switching between the two levels corresponds to real-time quantum jumps between singlet and triplet system. The collected photons originate from repetitive transitions between the singlet ground and excited states ($S_0 \Leftrightarrow S_1$,) giving rise to emission. While being excited an electronic spin flip may occur, resulting in intersystem crossing (ISC) from S_1 to the lowest triplet state (T_1). The singlet–triplet crossing chance per excitation cycle is small. For the same reason the T_1 lifetime is relatively long, which causes an interruption of fluorescence as long as T_1 remains occupied. After decaying to the ground singlet state the $S_0 \Leftrightarrow S_1$ excitation–emission cycle restarts. Thus the fluorescence photons are emitted in bunches separated by dark periods that occur when the molecule is in T_1: so-called photon bunching.[74–76] Obviously fast integration of the fluorescence photons over time intervals shorter than the duration of the dark periods is essential to identify the time length of each excursion to T_1. Figure 3(b) shows a total observation interval of 3.5 s of the same $DiIC_{18}$ molecule, in image representation. The image displays clearly the stochastic character of the on/off switching, especially due to the large dynamic range (five orders-of-magnitude) which allows identification of thousands of triplet excursions. Throughout the 3.5 s the $DiIC_{18}$ molecule spends about one quarter of its time in the dark T_1 state, a clear indication of the excitation condition close to the triplet limited saturation level. The combined ''light'' intervals over 3.5 seconds account for 1.9×10^6 counts, corresponding to $\sim 1.9\times10^7$ emitted photons.

From the real-time fluorescence data statistical values can be determined: the T_1 state decay time (τ_T) and the intersystem crossing yield (Y_{ISC}). Figure 4(a) shows the distribution of the length of all dark periods within the observation time, in a histogram. The distribution displays an exponential decay with 216(5) μs decay time. The monoexponential behavior prooves that the decay time is characteristic for the lifetime of the dark state, i.e., the triplet state lifetime (τ_T) of this specific molecule. Using the same data, the distribution of the number of photons in all light periods can be plotted. Again a monoexponential decay is obtained, from which an intersystem crossing yield $Y_{\mathrm{ISC}} = 3.6(5)\times10^{-4}$ is deduced, i.e., the chance per excitation that this specific molecule makes a transition to the triplet system. Figure 4(b) shows a dark period distribution for another molecule in the same sample. Here two observations are notable. First, the decay is again monoexponential, however with a triplet lifetime τ_T of 590(30) μs, more than twice the value for the molecule in Fig. 4(a). Second, the distribution has long tail of individual events of long dark intervals. For example, a dark interval of 8 ms occurs, far beyond the statistical probability for a triplet excursion. In many molecules we have observed dark intervals of $\sim$100 ms and even seconds, which definitely implies an origin different from intersystem crossing.

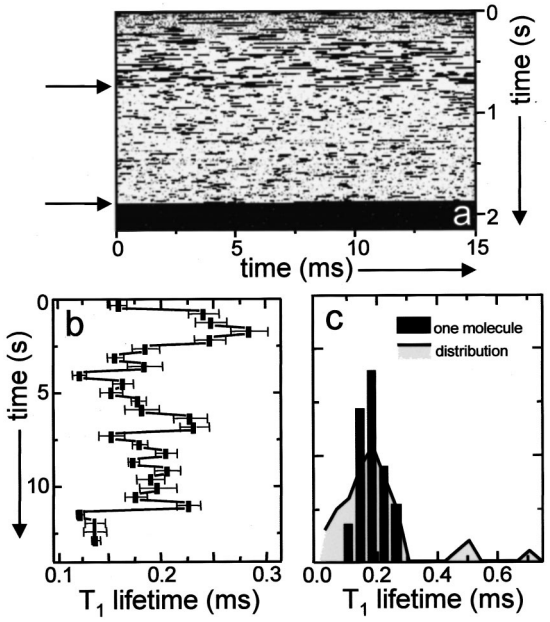

FIG. 5. (a) Time-image of fluorescence blinking with abrupt photodissociation after 1.877 s of excitation (arrow). The intersystem crossing dynamics changes abruptly after 0.70 s (arrow). (b) Trajectory of T_1 lifetime variation for an individual $DiIC_{18}$ molecule in PMMA as a function of time until its photodissociation after 13 s. (c) Histograms of the relative occurrence of the T_1 lifetimes for the single molecule in (b) (bars), and distribution of T_1 lifetimes for 51 spatially dispersed individual molecules in PMMA (line). Clearly the role of time and space is similar in determining the lifetime variation.

The fluorescence time traces of 80 $DiIC_{18}$ molecules in a PMMA host were recorded until photodissociation occurred. Remarkably, upon analysis, for 28 molecules the dark and light distributions showed deviations from a simple monoexponential decay, indicating rather multiexponential decay. Figure 5(a) shows the real-time dynamics of such a molecule, abruptly terminated by photodissociation after 1.877 s of excitation. A close look at the light/dark pattern immediately reveals a sudden change in the ISC dynamics after 0.70 s of excitation: the dark periods become significantly shorter. Apparently τ_T (and Y_{ISC}) is not constant in time, which directly explains the deviation from a monoexponential decay over longer observation time. Discrete jumps in triplet lifetime have also been observed by Ha *et al.*[75] and Weston *et al.*[76] using confocal microscopy. The lifetime variation is a signature of the fluctuation of the local environment, similar to the case of spectral diffusion.[24–26] A statistically relevant lifetime τ_T value can only be associated to observation time intervals shorter than the characteristic time scale of the fluctuations. To take the variation into account we have determined τ_T over sequential time intervals. The time windows should contain sufficient dark intervals for accurate determination of τ_T. Typically 2000 triplet excursions per second are observed, given our high count rate and short integration time. We have taken a time window of 400 ms, yielding an accuracy of at least 20 μs in the τ_T value. Figure 5(b) shows the trajectory of τ_T for a single molecule as a function of the observation time. Triplet lifetime fluctuations between 0.12 to 0.28 ms on a characteristic time scale of a few seconds are observed, until irreversible photodissociation occurs after 13 s. Throughout the trajectory the molecule visits the triplet state 21×10^3 times and emits $\sim7\times10^7$ photons. The relative occurrence of the different τ_T values over the entire observation period has been plotted in a histogram in Fig. 5(c). Note: this is a histogram for only one molecule. For other ''lifetime variable'' molecules similar histograms have been constructed that cover the same τ_T range. While sliding the 400 ms window over the fluorescence time trace both abrupt [Fig. 5(a)] and gradual changes in τ_T value are observed. Often photodissociation is limiting the buildup of a full single molecule histogram.

Reconsidering now the molecules with monoexponential decay, this simply indicates that τ_T (and Y_{ISC}) was constant during the entire observation time. All these ''constant'' molecules, each with their τ_T at their specific location, constitute a spatial distribution of τ_T values. In Fig. 5(c) the distribution of τ_T for 51 molecules is superimposed on the histogram for one molecule. The distribution peaks at 170 μs, exactly coinciding with the peak value for the time variable molecule. Similarly the width of the spatial τ_T distribution coincides with the lifetime values visited in time by one molecule. Clearly, after about 10 s of observation the distribution of T_1 lifetimes of one molecule becomes similar to the distribution obtained from many spatially dispersed molecules during short observation time. This observation confirms the validity of the ergodic theorem for this system: heterogeneity in time and space is of the same nature. Yet some molecules in the far tail of the distribution have long triplet lifetimes, which we did not observe in time trajectories. Probably these molecules reside at specific sites in the polymer host, e.g., in a void protected against oxygen quenching.

Time variation of photodynamical parameters, as observed for intersystem crossing, can be understood if one considers that the polymer host at room temperature constitutes a semirigid dynamic environment.[17,25] For example, local conformational dynamics of the polymer host[77] can modulate the oxygen concentration and diffusion on molecular scale, which in turn will influence the triplet parameters. Gradual and abrupt changes in the ISC dynamics might be associated to polymer mobility and fluorophore rearrangement, respectively.

In conclusion, near-field excitation of individual emitters allows to probe the spatial and temporal dynamics of the local environment on a truly nanometric scale with microsecond real-time resolution. The presented time-varying photodynamics demonstrates the potential of single molecule detection to establish a relation between the inhomogeneity of the ensemble and the real-time dynamics of the heterogeneity of the environment.

DENDRITIC MACROMOLECULES

A much higher degree of control of the local nanoenvironment can be obtained through macromolecular engineering: following nanochemistry synthesis routes, molecular building blocks can be connected to constitute a complex shell structure of nanometer dimensions.[78] In this study we have chosen for dendritic molecules containing a single fluorescent Rhodamine B (RhB) chromophore as a first test case

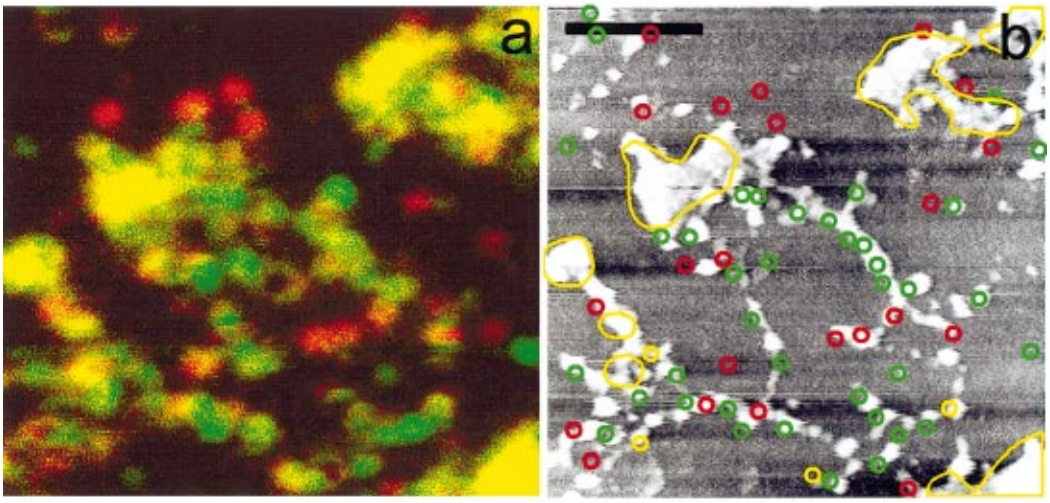

FIG. 6. (Color) (a) Near-field fluorescence image of individual dendritic molecules, with ~70 nm optical resolution. Scan range $1.65\times1.65\ \mu m^2$ at 1 ms/pixel. The excitation light at $\lambda = 514.5$ nm is circularly polarized. Fluorescence signal is typically 50 kcounts/pixel for an isolated spot. The fluorescence signal is color-coded red/green according to the detected x/y polarization, and thus indicating the in-plane orientation of the molecular emission dipole. (b) Simultaneously obtained shear-force image showing both isolated and clustered dendritic molecules on the glass surface. Contours of the fluorescence spots and clusters in (a) are overlayed to facilitate colocalization of fluorescence and topography. Both correlated and noncorrelated spots are observed, indicating presence of dendritic molecules with fluorescent core, without fluorescent core, and isolated fluorophores. Scalebar: 450 nm.

for near-field optical single molecule detection. Dendritic molecules are regular hyperbranched polymers, which originate from a nucleus by means of repetitive reaction.[79] The repetitive attachment of building blocks allows controlled dimensions from a few to hundreds of nanometers and offers ample opportunity to attach functional groups in well-defined three-dimensional architectures. Observation of single dendrimers with a fluorescent core embedded in a thin polystyrene film was recently reported by Hofkens *et al.*[80] using confocal microscopy. We have directed our attention to single dendritic molecules adsorbed on a glass surface because the near-field method yields the unique opportunity to correlate single molecular fluorescence with the topography of an individual dendritic molecule on the surface. Furthermore we show that polarization sensitive detection can be exploited to distinguish individual dendritic molecules from a cluster. Obviously the dipole moments of the fluorescent cores in a cluster will be randomly oriented, in contrast to the defined orientation of individual molecules.

Synthesis of the dendritic structures was based on coordination chemistry using organo-palladium building blocks, as previously shown.[81] Each building block allows attachment of two new building blocks, using coordination to the fourth position of the palladium. Thus higher generations dendritic spheres are obtained with a final dimension controlled by the size of the counter-ion used in the solvent.[82] To assemble single chromophoric structures RhB functionalized organo-palladium building blocks were added to the solution in a 1:14 ratio. With this ratio a majority of third-generation structures is expected, containing only one RhB core per molecule.

Size and polydispersity of the synthesized spheres were verified by tapping mode atomic force microscopy of individual dendritic molecules, spin-coated on glass. The height distribution of the dendritic molecule spheres was found to peak at 7.5(5) nm, which indeed matches a third-generation assembly. Yet the width of the distribution [FWHM 5.0(5) nm], indicates also dendritic structures of lower and higher generation.

Figure 6(a) displays a near-field fluorescence measurement of a $1.65\times1.65\ \mu m^2$ area of the dendritic sample, as spin-coated on glass. The incident light at 514 nm was circularly polarized. Fluorescence was filtered using a 550 nm long-pass filter and collected over 1.3 NA in two perpendicular polarization channels. A fluorescence signal of typically 50 kcounts/s was detected from an individual RhB core molecule. The pseudocolors in the image correspond to the polarization direction of the detected fluorescence, ranging from green (polarization in the vertical image direction) via yellow (equal vertical and horizontal components) to red (horizontal polarization). Many individual spots with well-defined polarized emission are observed, i.e., with one fixed dipolar emission moment. We identify all these isolated fluorescence spots as single dendritic molecules. This identification is further supported by the observation of discrete on–off blinking of the fluorescence on a millisecond to second time scale and the abrupt termination of the emission after repeated scans (probably photodissociation). Also the fluorescence signal is of the same order-of-magnitude as the signal obtained of single $DiIC_{18}$ molecules using the same near-field probe. The ring-shaped molecule in the center of the image is a typical near-field optical signature of a perpendicularly oriented absorption dipole. The inner diameter of the ring-like spot is 70 nm, in accordance with the expectation for a 70 nm aperture at a distance of 15 nm.[49,72] Apart from the isolated spots representing individual emitters, larger agglomerates can be distinguished with an overall yellow color, i.e., equal polarization components in both channels. In these dendritic clusters, several RhB molecules are excited simultaneously resulting in randomized polarization and a higher signal level than for the isolated spots. The cluster emission is practically independent of the excitation

polarization conditions. Nevertheless, some individual molecules can still be distinguished at the edges of the cluster areas due to the small illumination volume of the probe.

Simultaneously with the near-field fluorescence image a shear-force height measurement was obtained [Fig. 6(b)]. Both isolated and agglomerated spheres are visible in the image. The isolated spheres have lateral dimensions down to 20 nm, whereas the lateral cluster size ranges up to several hundreds of nm. Within the clusters, individual spheres can be resolved with 20–70 nm lateral dimensions. The 20 nm lateral resolution is limited by convolution with a small particle at the tip end. The height of the spheres is between 5 and 7 nm. The good agreement with the height distribution found by tapping mode AFM is remarkable as the actual tip-sample interaction, and hence the contrast mechanism, is different between shear force and tapping mode force microscopy.

To facilitate a better image analysis, contours of the fluorescence spots and clusters as determined from Fig. 6(a) are superimposed on top of the topography in Fig. 6(b). The strong correlation between spheres and clusters and the presence of fluorescence is obvious. Indeed the dendritic molecule clusters correspond to the unpolarized agglomerates. However, upon closer inspection one finds that some spherical particles in the topographic image do not exhibit any fluorescence. Definitely all chromophores are excited using our FIB modified probe with circular excitation polarization, as it ensures the presence of an optical field component in all spatial directions. As a consequence the absence of fluorescence for some dendritic molecules must be attributed to the absence of a chromophore core altogether or to a chromophore core in a nonfluorescent state. Definitely photodissociation, as observed on repeated scanning, is the main cause for the lack of fluorescence. Yet, even at initial scanning often a fraction of dentritic molecules was nonfluorescent. Conversely, some fluorescent spots in the optical image do not correspond to any detectable height features in the topographic image [Fig. 6(b)]. The shear force feedback mechanism in these experiments yields a corresponding noise of 0.3 nm in topography. A feature should be appreciably smaller than 1 nm to give no detectable topography. Therefore we attribute the fluorescent sites to unreacted core molecules, i.e., the first dendritic generation that is too small to be detected by the shear force mechanism. Clearly the sensitive photon-counting fluorescence detection allows recognition of molecules where force detection fails to discern them.

Interestingly, the presence of unreacted first generation core molecules and fully assembled third-generation dendritic molecules allows a direct comparison of their photophysical behavior. Yet, for these particular dendritic structures, we find no significant differences in fluorescence signal, blinking, and dissociation behavior. Apparently the photophysics of the fluorescent core unit is not substantially altered upon assembly in the dendritic structure. By two-channel polarization detection, we did observe rotational movement of both free and assembled fluorescent cores on a millisecond time scale. It is unlikely that the entire molecular assembly is involved in the observed motions. In repeated force imaging no motion was observed. More likely the coordinated palladium bonds allow the fluorescent core certain motional degrees of freedom in its attachment to the dendritic shell. We attribute the rotational motion to the rattling of the RhB core unit within its surrounding dendritic host. In contrast, Hofkens *et al.*[80] reported rotational movement of single covalently bonded dendrimers embedded in a thin polystyrene film on a much longer timescale (>10 s), which was attributed to thermally induced polymer movements. The difference in environment and bonding type (coordination vs. covalent) can easily account for these differences.

Obviously the presented experiments are only a first step in the application of near-field single molecule detection to synthetic macromolecules. On the one hand the single molecule detection gives an ultimate analysis of the outcome of the synthetic ''bottom-up'' approach. On the other hand macromolecules can be dedicatedly engineered with sensing or switching capabilities, which form an attractive challenge to be addressed by the ''top-down'' near-field method.

SINGLE GREEN FLUORESCENT PROTEINS

The ultimate examples of mastering the molecular nanoenvironment are found in nature itself. For example, property and function of proteins is fully determined by highly optimized conformational structure and coordinated local chemistry. The efficient autofluorescence of the so-called green fluorescent protein (GFP) arises entirely from rigid conformational confinement. Over the last years the GFP has attracted great attention in molecular biology, because autofluorescence can be induced in many proteins by fusion to GFP, while the biological function of the protein is retained. Thus expression or transport can be monitored by fluorescence sensitive methods without the need of exogenous fluorescence dyes: a true *in vivo* marker.[83,84]

The GFP is a natural 238 amino acid ''guest–host system'' in the sense that the intrinsic chromophore is encapsulated in a perfect barrel-like structure: a cylinder consisting of eleven beta strings. Short alpha helix segments close the two ends and create a framework for the chromophore within the cylinder. The chromophore arises from the autocatalytic formation of a three amino acid sequence: Ser65-Tyr66-Gly76.[85] The rigid and total encapsulation of the chromophore is probably responsible for the high fluorescence quantum yield and reduced O_2 quenching. By exchanging specific amino acids (mutagenesis) the fluorescence intensity can be enhanced 10–30 times, compared to wild-type GFP.

The first observation of individual GFP fluorescence, by Dickson *et al.*,[86] immediately revealed discrete on/off switching and intensity fluctuation, with strong resemblance to the quantum jumps of organic dyes, however on a much longer time scale. The origin of the complex GFP photodynamical behavior is yet unclear.[87] In this study we have focussed on the S65T-GFP mutant, where Thr replaces the Ser65.[88] The S65T-GFP is efficiently excited at the 488 nm Ar^+-line, resulting in a narrow emission band around 508 nm. We have applied our near-field optical method to study the real-time fluorescence dynamics of S65T-GFP in more detail.[59]

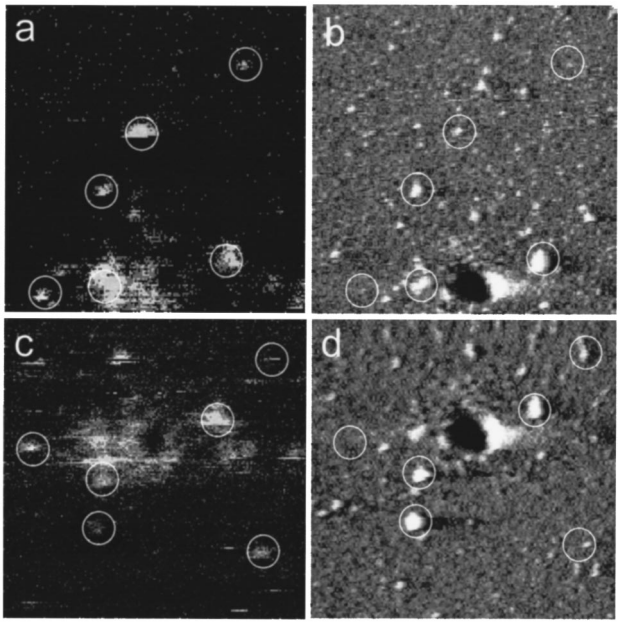

FIG. 7. Near-field optical images ($2\times2\ \mu m^2$) of individual S65T green fluorescent proteins (GFPs) on glass. (a), (c) Fluorescence of individual GFPs showing up as isolated spots (indicated by circles). Most GFPs switch abruptly on/off, resulting in partial images of one or a few lines. (b), (d) Corresponding topography, displaying the glass surface roughness and several individual GFPs of 2–4 nm height. Proteins corresponding in topography and fluorescence are indicated by circles.

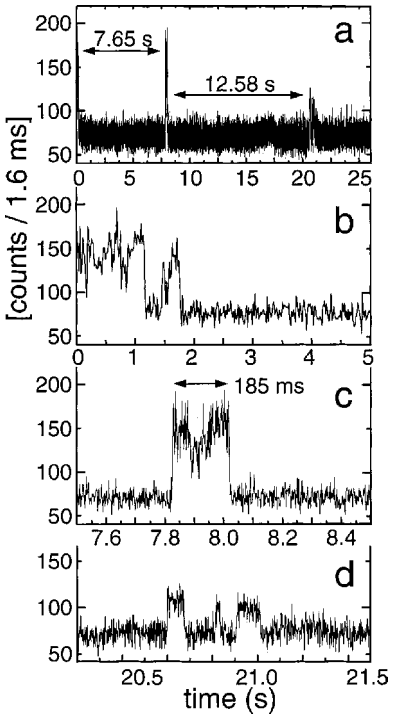

FIG. 8. Fluorescence signal of an individual S65T-GFP in time, during 26 s with 1.6 ms integration time, at 14 kW/cm^2 excitation intensity. (a) Total fluorescence time trace, showing mainly background signal with occasional GFP fluorescence bursts. (b), (c), (d) Magnification of the fluorescence bursts, containing a few thousand photocounts, during typically 100 ms.

The individual proteins were either adsorbed on glass to enable simultaneous topographic imaging, or embedded in water-pore gels to guarantee a hydrated environment. For adsorption to glass, a solution of S65T-GFP in Na phosphate buffer, pH 7.0, diluted to a final concentration of 5×10^{-8} M, was deposited on freshly cleaned hydrophilic glass and left to dry. The gel samples were prepared by immobilizing a 10^{-7} M solution of S65T-GFP in PBS in the water-filled pores of poly(acrylamide) gel. The gel was sandwiched between glass cover-slips and left to polymerize. The resultant gel film was around 3 μm thick with 3 nm pores, sufficient to spatially confine the proteins while retaining their native conformation.

Images of individual S65T-GFP molecules as freshly deposited on the glass surface are presented in Fig. 7. Near-field fluorescence and topography are simultaneously recorded over a scan area of $2\times2\ \mu m^2$ at an integration time of 3 ms/pixel. Isolated spots corresponding to the fluorescence emission of individual GFPs can be recognized in the optical images [Figs. 7(a), 7(c)]. The size of the individual fluorescence spots is 70 nm (FWHM). Most GFPs fluoresce only during a few scan lines. Some GFPs show up only as a few pixels on one line. The abrupt cease and start of emission is of course a clear indication for individual GFPs, but also for strongly dynamic behavior. Detection in both polarization channels shows that the emission from each spot has a defined polarization direction, again evidence for detection of individual GFPs. The fluorescent spots can be directly correlated to features in the topographic images [Figs. 7(b), 7(d)]. The size of the isolated protein features in the topographic images is 2–5 nm in height and approximately 10 nm in width for the smallest objects. The dimensions correspond well to the 4 nm size of the GFP barrel. Almost any single fluorescent spot has a corresponding topographic signature, as marked by the circles in the images. Yet, many of the topographic features do not have a corresponding fluorescent signature. These nonfluorescent features can be of different origin. They can be residual salt clusters from the buffer solution. Alternatively they can be incomplete or nonfully folded GFPs, which will appear on the topographic image but are nonfluorescent.[23,59] Finally, the proteins can be in a temporary nonemissive state during the time of imaging. Upon sequential imaging of the same area we find different proteins lightning up from image to image. Obviously the appearance of the fluorescence images is heavily affected by a dark state. We conclude that the majority of the objects in the topographic images are indeed proteins. In fact the simultaneous topographic and fluorescence detection could give information on the percentage of GFPs in a dark state or nonfully folded conformation.

In order to address the on/off switching in more detail, we have recorded real-time fluorescence time traces of individual S65T-GFPs. The GFPs were embedded in water-pore PAA gels to guarantee a more native environment. The experimental procedure is similar to the $DiIC_{18}$ investigations, presented before. Figure 8 displays part of a fluorescence trace recorded at 14 kW/cm^2 excitation intensity. The peak count rate of 6×10^4 counts/s is low compared to $DiIC_{18}$ under similar conditions, and forced us to extend the integration time to 1.6 ms for sufficient photon statistics. The time trace reveals directly that the GFP emission occurs in bursts

of fluorescence separated by long dark intervals of several seconds. Magnification of the bursts in Figs. 8(b), 8(c), and 8(d) shows that the bright intervals contain a few thousand counts, emitted typically during ~100 ms. The chance to observe a fluorescent S65T-GFP is only 5% under these conditions. The lack of fluorescent GFPs in Fig. 7 is a direct illustration of this low ''on'' chance. Obviously the long dark intervals have severe consequences for the applicability of the GFP as a biological marker in single molecule studies.

We find that the burst intensity is proportional to the excitation intensity, while the bright time interval reduces with increasing intensity. Therefore the off-switching process is photoinduced, very similar to intersystem crossing. The chance per excitation to reach the dark state is only $\sim 10^{-5}$. Yet the long-term stability of the dark state sets a severe limit to the attainable fluorescence signal. In practice the time averaged photon emission yield is below 10^5 photons/s.

The burst-like behavior of the GFP puts a special meaning to the issue of photodissociation. Occasionally a GFP gives merely one burst, usually it blinks on/off repeatedly, and sometimes it recovers and starts reemitting only after minutes. Apparently, even after a very long dark time the GFP has the ability to reconstitute its original fluorescent chromophoric conformation. The irregular behavior over a wide dynamic time range complicates the determination of the maximum number of emitted photons. We collected typically $\sim 10^5$ and occasionally $\sim 10^6$ photons from a single S65T-GFP.

The biological nature of the long-lived dark state is yet to be clarified. Triplet states can be ruled out as fluorescence correlation spectroscopy has recently shown that GFP triplet lifetimes are typically 5–25 μs.[89] According to Moerner *et al.*[87] the blinking is pH independent, which rules out reversible proton transfer mechanisms. Recently, in a theoretical approach, the existence of a ''dark'' zwitterionic intermediate form was predicted,[90] related to a *cis–trans* isomerization. Presumably reversible torsional motion within the chromophore is the cause for the long term on/off switching.

CONCLUSIONS

The quality and reproducibility of near-field optical methods has been largely enhanced by the introduction of high definition aperture probes, fabricated by focused ion beam milling. Apertures down to 20 nm have been realized, where a typical aperture of 70 nm gives up to 1 μW and a polarization extinction ratio $>$ 100:1 in the far-field. Single molecules have been imaged using the FIB probes. The improved imaging characteristics are demonstrated by the observed near-field patterns, where the single molecule probes the spatial and vectorial electric field distribution of the aperture, in agreement with calculations. It was shown that the orientation of molecular transition dipole moments could be determined by proper interpretation of the characteristic near-field excitation patterns, that arise due to the presence of both lateral and longitudinal polarized electric fields close to the aperture edge. Local optical field distributions with 45 FWHM have been observed. The confined optical field allows to discriminate molecules at distances below 10 nm, as compared to $>$ 40 nm in far-field methods.

The high local excitation intensity (up to 20 kW/cm^2) allowed us to record real-time fluorescence traces with μs time resolution. Discrete quantum jumps, due to intersystem crossing, were observed, displaying the real-time photodynamic response of the molecule to the fluctuations in the heterogeneity of its local environment. Triplet-state parameters were shown to vary on a time scale of seconds for $DiIC_{18}$ embedded in PMMA. The observed similarity between spatial and temporal distributions indicated that the environmental sites become indistinguishable from each other in time, i.e., the system is stationary.

Individual dendritic molecules containing a single fluorescent core (RhB) have been studied by near-field optical methods. Colocalization of single molecule fluorescence with the dendritic molecules was observed in simultaneous topographic and fluorescence images. Fluorescent assemblies could be discriminated from free fluorophores and nonfluorescent dendritic molecules. Orientational mobility of the core fluorophore within the dendritic host shell has been observed for the first time.

Finally, simultaneous topographic and fluorescence imaging of individual copies of the green fluorescent protein (S65T-GFP) was performed. Dramatic on/off blinking on long time intervals of seconds was observed. Fluorescence time traces displayed emission in short photon bursts. Transitions to the dark conformational state turned out to be photoinduced. The observation has important implications for the use of GFPs as an *in vivo* marker in molecular biology studies based on single molecule analysis.

ACKNOWLEDGMENTS

This work is financially supported by the Netherlands Foundation for Fundamental Research of Matter (FOM) and the NanoLink orientation of the MESA$^+$ Research Institute. The research of M.F.G.-P. has been made possible by a fellowship of the Royal Netherlands Academy of Arts and Sciences (KNAW). The authors are grateful to S. A. Levi, F. C. J. M. van Veggel, and D. N. Reinhoudt (Supra-Molecular Chemistry & Technology, University of Twente) for synthesis, characterization, and availability of the RhB-dendritic molecules. V. Subramaniam and Th. Jovin (Max Plank Institute, Biophysical Chemistry, Göttingen, Germany) are acknowledged for the purified S65T-GFPs used in this work. Finally we would like to thank J. Korterik, S. J. T. van Noort, K. O. van der Werf, A. M. Otter, F. B. Segerink, W. H. J. Rensen, A. van Zwol, G. M. J. Segers-Nolten, and B. G. de Grooth for their assistance and constructive suggestions.

[1] E. Betzig and R. J. Chichester, Science **262**, 1422 (1993).
[2] W. E. Moerner and L. Kador, Phys. Rev. Lett. **62**, 2535 (1989).
[3] M. Orrit and J. Bernard, Phys. Rev. Lett. **65**, 2716 (1990).
[4] S. Nie, D. T. Chiu, and R. N. Zare, Science **266**, 1018 (1994).
[5] M. Eigen and R. Rigler, Proc. Natl. Acad. Sci. USA **91**, 5740 (1994).
[6] T. Funatsu, Y. Harada, M. Tokunaga, K. Saito, and T. Yanagida, Nature (London) **374**, 555 (1995).
[7] *Single Molecule Optical Detection Imaging, and Spectroscopy*, edited by

T. Basché, W. E. Moerner, M. Orrit, and U. P. Wild (VCH, Weinheim, Germany, 1997).
[8] W. E. Moerner, Acc. Chem. Res. **26**, 563 (1996).
[9] X. S. Xie, Acc. Chem. Res. **26**, 598 (1996).
[10] P. M. Goodwin, W. P. Ambrose, and R. A. Keller, Acc. Chem. Res. **26**, 607 (1996).
[11] X. S. Xie and J. K. Trautman, Annu. Rev. Phys. Chem. **49**, 441 (1998).
[12] W. E. Moerner and M. Orrit, Science **283**, 1670 (1999).
[13] Frontiers in Chemistry: Single Molecules, topical issue, Science **283**, 1593 (1999).
[14] Th. Schmidt, G. J. Schütz, W. Baumgartner, H. J. Gruber, and H. Schindler, J. Phys. Chem. **99**, 17662 (1995).
[15] M. A. Bopp, A. J. Meixner, G. Tarrach, I. Zschokke-Granacher, and L. Novotny, Chem. Phys. Lett. **263**, 721 (1996).
[16] R. M. Dickson, D. J. Norris, Y. L. Tzeng, and W. E. Moerner, Science **274**, 966 (1996).
[17] A. G. T. Ruiter, J. A. Veerman, M. F. Garcia-Parajo, and N. F. van Hulst, J. Phys. Chem. A **101**, 7318 (1997).
[18] R. D. Vale, T. Funatsu, D. W. Pierce, L. Romberg, Y. Harada, and T. Yanagida, Nature (London) **380**, 451 (1996).
[19] K. Kitamura, M. Tokunaga, A. H. Iwane, and T. Yanagida, Nature (London) **397**, 129 (1999).
[20] Y. Harada, T. Funatsu, K. Murakami, Y. Nonoyama, A. Ishihama, and T. Yanagida, Biophys. J. **76**, 709 (1999).
[21] T. Ha, Th. Enderle, D. S. Chemla, P. R. Selvin, and S. Weiss, Phys. Rev. Lett. **77**, 3979 (1996).
[22] T. Ha, J. Glass, Th. Enderle, D. S. Chemla, and S. Weiss, Phys. Rev. Lett. **80**, 2093 (1998).
[23] M. F. Garcia-Parajo, J. A. Veerman, J. van Noort, B. G. de Grooth, J. Greve, and N. F. van Hulst, Bioimaging **6**, 43 (1998).
[24] J. K. Trautman, J. J. Macklin, L. E. Brus, and E. Betzig, Nature (London) **369**, 40 (1994).
[25] J. J. Macklin, J. K. Trautman, T. D. Harris, and L. E. Brus, Science **272**, 255 (1996).
[26] H. P. Lu and X. S. Xie, Nature (London) **385**, 143 (1997).
[27] W. P. Ambrose, P. M. Goodwin, J. C. Martin, and R. A. Keller, Science **265**, 364 (1994).
[28] X. S. Xie and R. C. Dunn, Science **265**, 361 (1994).
[29] R. X. Bian, R. C. Dunn, X. S. Xie, and P. T. Leung, Phys. Rev. Lett. **75**, 4772 (1995).
[30] L. Novotny, Appl. Phys. Lett. **69**, 3806 (1996).
[31] L. Edman, U. Mets, and R. Rigler, Proc. Natl. Acad. Sci. USA **93**, 6710 (1996).
[32] Y. Jia, A. Sytnik, L. Li, S. Vladimirov, B. S. Cooperman, and R. M. Hochstrasser, Proc. Natl. Acad. Sci. USA **94**, 7932 (1997).
[33] M. Sauer, K. H. Drexhage, U. Lieberwirth, R. Müller, S. Nord, and C. Zander, Chem. Phys. Lett. **284**, 153 (1998).
[34] T. Ha, A. Y. Ting, J. Liang, W. B. Caldwell, A. A. Deniz, D. S. Chemla, P. G. Schultz, and S. Weiss, Proc. Natl. Acad. Sci. USA **96**, 893 (1999).
[35] S. Weiss, Science **283**, 1676 (1999).
[36] M. Wu, P. M. Goodwin, W. P. Ambrose, and R. A. Keller, J. Phys. Chem. **100**, 17406 (1996).
[37] D. A. vanden Bout, W. T. Yip, D. Hu, D. K. Fu, T. M. Swager, and P. F. Barbara, Science **277**, 1074 (1997).
[38] M. A. Bopp, Y. Jia, L. Li, R. J. Cogdell, and R. M. Hochstrasser, Proc. Natl. Acad. Sci. USA **94**, 10630 (1997).
[39] L. Ying and X. S. Xie, J. Phys. Chem. B **102**, 10399 (1998).
[40] Q. F. Xue and E. S. Yeung, Nature (London) **373**, 681 (1995).
[41] H. P. Lu, L. Xun, and X. S. Xie, Science **282**, 1877 (1998).
[42] J. Mertz, C. Xu, and W. W. Webb, Opt. Lett. **20**, 2532 (1995).
[43] E. J. Sanchez, L. Novotny, G. R. Holtom, and X. S. Xie, J. Phys. Chem. **101**, 7019 (1997).
[44] H. Yokota, K. Saito, and T. Yanagida, Phys. Rev. Lett. **80**, 4606 (1998).
[45] S. Nie and S. R. Emory, Science **275**, 1102 (1997).
[46] K. Kneipp, Y. Wang, H. Kneipp, L. T. Perelman, I. Itzkan, R. R. Dasari, and M. S. Field, Phys. Rev. Lett. **78**, 1667 (1997).
[47] A. M. van Oijen, J. Köhler, J. Schmidt, M. Müller, and G. J. Brakenhoff, Chem. Phys. Lett. **292**, 183 (1998).
[48] J. A. Veerman, A. M. Otter, L. Kuipers, and N. F. van Hulst, Appl. Phys. Lett. **72**, 3115 (1998).
[49] J. A. Veerman, M. F. Garcia-Parajo, L. Kuipers, and N. F. van Hulst, J. Microsc. **194**, 477 (1999).
[50] B. Hecht, H. Bielefeld, L. Novotny, Y. Inouye, and D. W. Pohl, Phys. Rev. Lett. **77**, 1889 (1996).
[51] E. Betzig, R. J. Chichester, F. Lanni, and D. L. Taylor, Bioimaging **1**, 129 (1993).
[52] M. H. P. Moers, W. H. J. Kalle, A. G. T. Ruiter, J. C. A. G. Wiegant, A. K. Raap, J. Greve, B. G. de Grooth, and N. F. van Hulst, J. Microsc. **182**, 40 (1996).
[53] Th. Enderle, T. Ha, D. F. Ogletree, D. S. Chemla, C. Magowan, and S. Weiss, Proc. Natl. Acad. Sci. USA **94**, 520 (1997).
[54] N. F. van Hulst, M. F. Garcia-Parajo, M. H. P. Moers, J. A. Veerman, and A. G. T. Ruiter, J. Struct. Biol. **119**, 222 (1997).
[55] E. Mei and D. A. Higgins, Appl. Phys. Lett. **75**, 430 (1999).
[56] S. A. Vickery and R. C. Dunn, Biophys. J. **76**, 1812 (1999).
[57] T. Ha, Th. Enderle, D. F. Ogletree, D. S. Chemla, P. R. Selvin, and S. Weiss, Proc. Natl. Acad. Sci. USA **93**, 6264 (1996).
[58] M. F. Garcia-Parajo, J. A. Veerman, A. G. T. Ruiter, and N. F. van Hulst, Ultramicroscopy **71**, 311 (1998).
[59] M. F. Garcia-Parajo, J. A. Veerman, G. M. J. Segers-Nolten, B. G. de Grooth, J. Greve, and N. F. van Hulst, Cytometry **36**, 239 (1999).
[60] D. W. Pohl, W. Denk, and A. Lanz, Appl. Phys. Lett. **44**, 651 (1984).
[61] E. Betzig and J. K. Trautman, Science **257**, 189 (1992).
[62] M. A. Paesler and P. J. Moyer, *Near-field Optics: Theory, Instrumentation, and Applications* (Wiley, New York, 1996).
[63] E. Betzig, J. K. Trautman, T. D. Harris, J. S. Weiner, and R. L. Kostelak, Science **251**, 1468 (1991).
[64] G. A. Valaskovic, M. Holton, and G. H. Morrison, Appl. Opt. **34**, 1215 (1995).
[65] K. Karrai and R. D. Grober, Appl. Phys. Lett. **66**, 1842 (1995).
[66] A. G. T. Ruiter, J. A. Veerman, K. O. van der Werf, and N. F. van Hulst, Appl. Phys. Lett. **71**, 28 (1997).
[67] A. G. T. Ruiter, K. O. van der Werf, J. A. Veerman, M. F. Garcia-Parajo, W. H. J. Rensen, and N. F. van Hulst, Ultramicroscopy **71**, 149 (1998).
[68] W. H. J. Rensen, N. F. van Hulst, A. G. T. Ruiter, and P. E. West, Appl. Phys. Lett. **75**, 1640 (1999).
[69] D. Axelrod, Biophys. J. **26**, 557 (1979).
[70] C. J. Bouwkamp, Rep. Prog. Phys. **17**, 35 (1954).
[71] L. Novotny, D. W. Pohl, and B. Hecht, Opt. Lett. **20**, 970 (1995).
[72] J. A. Veerman, M. F. Garcia-Parajo, L. Kuipers, and N. F. van Hulst (unpublished).
[73] J. A. Veerman, M. F. Garcia-Parajo, L. Kuipers, and N. F. van Hulst, Phys. Rev. Lett. **83**, 2155 (1999).
[74] T. Basché, S. Kummer, and C. Bräuchle, Nature (London) **373**, 132 (1995).
[75] T. Ha, Th. Enderle, D. S. Chemla, P. R. Selvin, and S. Weiss, Chem. Phys. Lett. **271**, 1 (1997).
[76] K. D. Weston, P. J. Carson, J. A. DeAro, and S. K. Buratto, Chem. Phys. Lett. **308**, 58 (1999).
[77] K. Schmidt-Rohr, A. S. Kulik, H. W. Beckham, A. Ohlemacher, U. Pawelzik, C. Boeffel, and H. W. Spiess, Macromolecules **27**, 4733 (1994).
[78] G. A. Ozin, Adv. Mater. **4**, 612 (1992).
[79] W. T. S. Huck, F. C. J. M. van Veggel, and D. N. Reinhoudt, Angew. Chem. Int. Ed. Engl. **35**, 1213 (1996).
[80] J. Hofkens, R. Verheijen, R. Shukla, W. Dehaen, and F. C. de Schryver, Macromolecules **31**, 4493 (1998).
[81] W. T. S. Huck, F. C. J. M. van Veggel, B. L. Kropman, D. H. A. Blank, E. G. Keim, M. M. A. Smithers, and D. N. Reinhoudt, J. Am. Chem. Soc. **117**, 8293 (1995).
[82] W. T. S. Huck, B. A. Snellink-Ruël, F. C. J. M. van Veggel, J. W. Th. Lichtenberg, and D. N. Reinhoudt, Chem. Commun. (Cambridge) **1**, 1359 (1997).
[83] *Green Fluorescent Protein, Properties, Applications and Protocols*, edited by M. Chalfie and S. Kain (Wiley, New York, 1998).
[84] A. B. Cubitt, R. Heim, S. R. Adams, A. E. Boyd, L. A. Gross, and R. Y. Tsien, TIBS **20**, 448 (1995).
[85] R. Heim, D. C. Prasher, and R. Y. Tsien, Proc. Natl. Acad. Sci. USA **91**, 12501 (1994).
[86] R. M. Dickson, A. B. Cubitt, R. Y. Tsien, and W. E. Moerner, Nature (London) **388**, 355 (1997).
[87] W. E. Moerner, E. J. G. Peterman, S. Brasselet, S. Kummer, and R. M. Dickson, Cytometry **36**, 232 (1999).
[88] R. Heim, A. B. Cubitt, and R. Y. Tsien, Science **373**, 663 (1995).
[89] A. J. W. G. Visser and M. A. Hink, J. Fluoresc. **9**, 81 (1999).
[90] W. Weber, V. Helms, J. A. McCammon, and P. W. Langhoff, Proc. Natl. Acad. Sci. USA **96**, 6177 (1999).